

The dependence of mass energy absorption coefficient ratios on beam size and depth in a phantom

J. R. Cunningham and M. Woo

Physics Division, The Ontario Cancer Institute, Toronto, and Department of Medical Biophysics, University of Toronto, Ontario, Canada

D. W. O. Rogers and A. F. Bielajew

Ionizing Radiation Standards Section, National Research Council, Ottawa, Ontario, Canada

(Received 6 January 1986; accepted for publication 19 February 1986)

The Monte Carlo computer code "electron gamma shower" (EGS) has been used to determine photon spectra in a water phantom. Spectra used by Johns and Cunningham and for the AAPM dosimetry protocol have been used as input data and ratios of average mass energy absorption coefficients have been calculated for a number of depths and field sizes. The results show that there is a slight dependence on both of these parameters. For example, $(\bar{\mu}_{\text{en}}/\rho)_{\text{graphite}}^{\text{water}}$ for cobalt-60 varies from a value of 1.111 for the primary spectrum in air, to 1.135 at a depth of 20 cm in a phantom for a beam approximately 1 m² in area. This variation of over 2% is relevant for dosimetry. The variation is less than this for high-energy radiation beams and in most cases can be ignored. The effect is greater for high atomic materials such as bone, where the range of variation of $(\bar{\mu}_{\text{en}}/\rho)_{\text{water}}^{\text{bone}}$, again for cobalt radiation, may be as great as 15%. This too is less for high-energy bremsstrahlung spectra.

INTRODUCTION

In the determination of absorbed dose at a point in a photon beam from ionization chamber measurements, a number of multiplying factors must be used. These are derived and discussed elsewhere.²⁻⁵ Several of them are averaged quantities, averaged in principle, over the spectrum of photon energies present at the point. The details of the photon spectrum are rarely known, however, and assumptions and approximation procedures must be used. It must be expected that the photon spectrum at a point *P* in a phantom is altered by changing the size of the volume irradiated and the depth of the point *P* below the surface and this must be expected to have an effect on some of the dosimetry factors. In this paper we choose one of the factors, the "ratio of averaged mass energy absorption coefficients," and examine how it is affected by these conditions. This quantity was chosen for examination because it was expected to be one of the most likely to be affected by these conditions and it has not, to our knowledge, been examined in this way before.

The mass energy absorption coefficient (μ_{en}/ρ) plays a central role in photon dosimetry because it quantifies the energy transfer from the ionizing radiation to the medium. In more precise terms, it relates the photon fluence $\phi(h\nu)$ to the collision kerma $K_{c,m}$ in a material *m* by the relation

$$K_{c,m} = \phi(h\nu) [\mu_{\text{en}}(h\nu)/\rho]_m h\nu. \quad (1)$$

If a spectrum of photon energies is present, the kerma will be the sum of the kermas for each energy component,

$$K_{c,m} = \int_{h\nu} \left[\frac{d\phi(h\nu)}{dh\nu} \right] h\nu \left[\frac{\mu_{\text{en}}(h\nu)}{\rho} \right]_m dh\nu. \quad (2)$$

It is rare, in practice, that detailed information about the spectrum is available and assumed average values for these quantities are used. The custom is to calibrate a users' ionization chamber against a standard instrument. This is done by

a standardization laboratory where most commonly the reference exposure is established from a series of measurements made with a graphite ionization chamber in a ⁶⁰Co beam. Exposure is then determined from

$$X = J_{\text{air}} \frac{1}{k} \left(\frac{\bar{L}}{\rho} \right)_{\text{air}}^{\text{gr}} \left(\frac{\bar{\mu}_{\text{en}}}{\rho} \right)_{\text{gr}}^{\text{air}} \beta^{-1} \pi_i K_i, \quad (3)$$

where J_{air} is the charge per unit mass (C kg⁻¹) of air in the ion chamber, $k = 2.58 \times 10^{-4}$ C kg⁻¹ R⁻¹, $(\bar{L}/\rho)_{\text{air}}^{\text{gr}}$ is the ratio of averaged restricted collision mass stopping powers for graphite to air, $(\bar{\mu}_{\text{en}}/\rho)_{\text{gr}}^{\text{air}}$ is the ratio of average mass energy absorption coefficients for air to graphite, β is the quotient of absorbed dose and the collision part of the kerma, and $\pi_i K_i$ is a product of factors that account for small corrections that will not be discussed here.

For the exposure calibration, the value of $(\bar{\mu}_{\text{en}}/\rho)$ to be used would be that for the in-air spectrum and since ⁶⁰Co radiation is virtually monoenergetic the appropriate value for $(\bar{\mu}_{\text{en}}/\rho)$ is well known.

The situation is not quite so simple for dose determination at a point in a phantom. The irradiation conditions for this are shown in Fig. 1, which depicts a photon beam irradiating a phantom of material *m*₁. A determination of the absorbed dose at point *P* would be made by placing a dosimeter, made of material *m*₂, at this point and from the reading of the dosimeter, calculating the dose to material *m*₁ at that point as if the dosimeter were not present. It would be³

$$D_{m_2} = M N_{\text{gas}} (\bar{L}/\rho)_{\text{gas}}^{m_2} P_{\text{ion}} P_{\text{repl}} P_{\text{wall}}, \quad (4)$$

where M is the reading of the dosimeter, N_{gas} is the cavity gas calibration factor,³ $(\bar{L}/\rho)_{\text{gas}}^{m_2}$ is the stopping power ratio as for Eq. (3), P_{ion} is a factor to correct the ion chamber reading for efficiency of ion collection, P_{repl} is a replacement factor to correct for the perturbing effect of the dosimeter (ma-

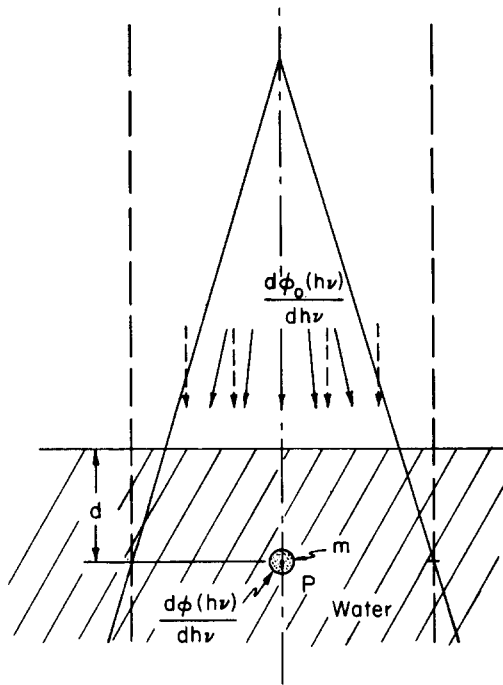


FIG. 1. Diagram showing a photon beam irradiating a water phantom in which a small mass of some other material, here labeled m is placed. The incident spectrum of photon energies is described by $d\phi_0(h\nu)/dh\nu$. This spectrum is altered by attenuation and scatter within the irradiated water and at the location of the insert is described by $d\phi(h\nu)/dh\nu$.

material m_2 replaces material m_1 , in the phantom), and P_{wall} is a factor to correct for the way the photons interact with m_2 compared to m_1 as follows:

$$P_{\text{wall}} = \frac{\alpha(\bar{L}/\rho)_{\text{gas}}^{m_2} (\bar{\mu}_{\text{en}}/\rho)_{m_2}^{m_1} + (1 - \alpha)(\bar{L}/\rho)_{\text{gas}}^{m_1}}{(\bar{L}/\rho)_{\text{gas}}^{m_1}}, \quad (5)$$

where α is the fraction of the ionization (M) produced by electrons arising from material m_2 (the wall of the ionization chamber) and $(1 - \alpha)$ is the fraction produced by electrons arising in the medium m_1 outside of the ion chamber. (\bar{L}/ρ) is, as before, a ratio of averaged stopping powers and $(\bar{\mu}_{\text{en}}/\rho)$ is the ratio of averaged mass energy absorption coefficients. If $(1 - \alpha)$ is small, as it is for photon energies of only a few MeV, then P_{wall} is almost proportional to the product of the ratio of mass stopping powers and the ratio of mass energy absorption coefficients. A preliminary examination of the dependence of both of these quantities on photon spectra strongly suggested that the absorption coefficient ratio is the more sensitive.

CALCULATIONS

The ratio of mass energy absorption coefficients is the ratio of the absorbed doses to the two materials that would result from the same photon spectrum interacting with each. This would also be the ratio of collision keramas,

$$\begin{aligned} \frac{D_{m_1}}{D_{m_2}} &\approx \frac{K_{m_1}}{K_{m_2}} = \frac{\int [d\phi(h\nu)/dh\nu] h\nu [\mu_{\text{en}}(h\nu)/\rho]_{m_1} dh\nu}{\int [d\phi(h\nu)/dh\nu] h\nu [\mu_{\text{en}}(h\nu)/\rho]_{m_2} dh\nu} \\ &= (\bar{\mu}_{\text{en}}/\rho)_{m_2}^{m_1}, \end{aligned} \quad (6)$$

where the integration is over all energies $h\nu$ in the photon fluence spectrum $d\phi(h\nu)/dh\nu$ at point P (Fig. 1) in a phantom of material m_1 .

This expression was used by Johns and Cunningham² to calculate ratios of averaged mass energy absorption coefficients for a number of combinations of materials for a number of spectra (Table 7.4, Ref. 2). This equation was also discussed by Cunningham and Schulz⁵ in connection with the preparation of data for the AAPM dosimetry protocol.³ The spectra that were used^{2,3} were taken either from the literature or were calculated, and with one exception were primary beam spectra, that is, they did not include phantom scatter. The exception was ^{60}Co for which a spectrum had been generated over 20 years ago by Bruce and Johns⁶ using Monte Carlo methods to describe photon spectra for a range of field sizes and depths in a water phantom.

RESULTS

Ratios of mean mass energy absorption coefficients were calculated using ^{60}Co primary photon energies only (1.17 and 1.33 MeV) and using the in-phantom Bruce and Johns spectrum for depth 20 cm and field size 20×20 cm and showed differences of about 0.5% for $(\bar{\mu}_{\text{en}}/\rho)_{\text{gr}}^{\text{water}}$. There were similar differences for other materials used in the construction of ionization chambers. For higher atomic number materials, such as bone, the differences produced by these different spectra are much greater and can easily exceed 5% for clinically relevant conditions. This observation led us to examine the behavior of this quantity using Monte Carlo calculations of spectra in phantoms.

^{60}Co radiation

Graphs of the part of the spectrum of radiation from a ^{60}Co source arising from photons scattered within a water phantom are shown in Fig. 2. Curve A in this diagram was obtained directly from Bruce and Johns,⁶ and represents the spectrum that exists at a point 10 cm deep in a 20×20 cm beam irradiating a phantom of infinite thickness. The graph is energy fluence plotted against photon energy. Curve B was obtained using electron gamma shower code (EGS)¹ for the same conditions as curve A. The agreement between the two is qualitatively good but there are some differences. Curve A was obtained using 2×10^4 photon histories and some analytical smoothing was used, while curve B was derived from 2×10^5 photon histories and is presented directly as obtained. It is made up from 400 energy intervals and the statistical variations can be inferred from the irregularities in the curve. We have shown the Bruce and Johns result because it provides a comparison with our work and there is a lack of reference data with which Monte Carlo calculations of this kind may be compared. We have assumed, however, that the EGS output is correct for what follows.

Both curves A and B of Fig. 2 were obtained using a single incident energy of 1.25 MeV. Curve C is the output of EGS using as input a photon spectrum which represents more realistically the beam from an actual cobalt treatment unit.⁷ This spectrum was generated by Rogers *et al.*,⁷ also using EGS. It consists of the primary plus a distribution of about 20% low-energy photons (energy fluence) generated within

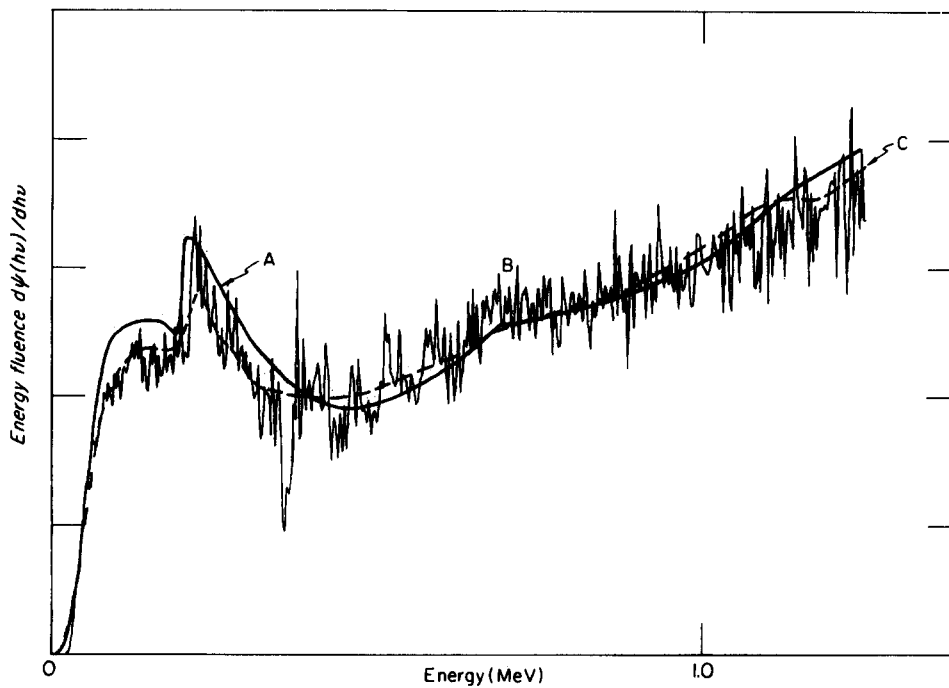


FIG. 2. Energy fluence spectrum for scattered radiation at a point *P* in a water phantom. The radiation is from a ⁶⁰Co source, the beam size is 20 × 20 cm at the phantom surface and point *P* is at a depth of 10 cm. Curve A is taken from Ref. 6. Curve B is calculated using the EGS code assuming incident photons of 1.25 MeV and curve C was calculated using EGS taking a spectrum generated by one of the authors (DWOR) to more realistically represent the spectrum from a Co source. It has been smoothed for display purposes.

the source or resulting from scatter from the collimator. The differences between curves B and C are significant only at the very low energy end of the curve where curve C has a small increase over B.

A user code was written for the EGS System (EGS3 as modified by Rogers⁸) and was implemented on a VAX 780 computer working under the operating system known as VMS. In order to make the calculations efficient, the inverse geometry described by Bruce and Johns⁶ was used. Using this procedure, data for several beam sizes and depths can be accumulated at the same time. The ratio of mean mass energy absorption coefficients is obtained from the ratio of the sums,

$$\left(\frac{\bar{\mu}_{en}}{\rho}\right)_{m_2}^{m_1} = \frac{\sum_{i=1}^n w_i (\mu_{en}/\rho)_{m_{1,i}} h\nu_i}{\sum_{i=1}^n w_i (\mu_{en}/\rho)_{m_{2,i}} h\nu_i}, \quad (7)$$

where the sum is over the number of photons that cross an area and the index *i* represents an individual photon history. *w_i* is 1/cos *θ_i*, where *θ_i* is the angle that the path of photon *i* makes with the normal to the area, *hν_i* is the photon's energy as it crosses, and (μ_{en}/ρ)_{*m_{1,i}*} and (μ_{en}/ρ)_{*m_{2,i}*} are the mass energy absorption coefficients for those photons in materials 1 and 2, respectively. The photon histories are generated in water and the weighted occurrence of photon energies at areas A defines the fluence spectrum. A record of the spectrum can be determined by keeping an account of the distribution of photon energies as they occur. This is plotted as curves B and C of Fig. 2 and in following diagrams.

Table I shows the results of evaluating Eq. (7) for cobalt radiation using the Rogers input spectrum for depths of 0, 5, 10, and 20 cm and beam radii representing beams that have areas 25, 100, and 400 cm², and infinity, respectively. The numbers in parentheses in the table are taken from Johns and Cunningham² (Table 7-4) representing the in-air and in-

TABLE I. Ratios of averaged mass energy absorption coefficients for ⁶⁰Co radiation for realistic input spectra.

	Beam area (cm ²)				
	0	25	100	400	∞
(a) water/graphite (1.111) (1.116) (1.111) ^a					
0	1.111	1.112	1.112	1.113	1.115
5	1.112	1.113	1.113	1.115	1.122
10	1.112	1.113	1.113	1.117	1.127
20	1.112	1.114	1.114	1.119	1.135
(b) water/PMMA (1.029) (1.032) (1.029) ^a					
0	1.029	1.030	1.030	1.030	1.031
5	1.029	1.030	1.030	1.032	1.036
10	1.029	1.030	1.030	1.033	1.040
20	1.029	1.031	1.031	1.034	1.045
(c) water/polystyrene (1.032) (1.037) (1.032) ^a					
0	1.032	1.033	1.033	1.033	1.036
5	1.032	1.034	1.034	1.036	1.044
10	1.033	1.034	1.034	1.038	1.050
20	1.033	1.035	1.035	1.041	1.059
(d) water/nylon (1.012) (1.017) (1.013) ^a					
0	1.013	1.013	1.013	1.014	1.016
5	1.013	1.014	1.014	1.016	1.022
10	1.013	1.015	1.015	1.018	1.027
20	1.013	1.015	1.015	1.020	1.034
(e) muscle/water (0.991) (0.992) (0.991) ^a					
0	0.991	0.991	0.991	0.991	0.992
5	0.991	0.991	0.991	0.992	0.992
10	0.991	0.991	0.991	0.992	0.993
20	0.991	0.991	0.991	0.992	0.993
(f) bone/water (0.954) (0.995) (0.955) ^a					
0	0.958	0.961	0.961	0.967	0.984
5	0.960	0.968	0.968	0.987	1.037
10	0.962	0.973	0.973	1.000	1.076
20	0.963	0.979	0.979	1.017	1.134

^aThe first term in parentheses is for in-air, the second term is for the depth = 10 cm, 20 × 20 cm field (Table 7-4, Ref. 2). The third is for the Rogers's (Ref. 7) realistic spectrum in air.

phantom spectra and the in-air realistic spectrum of Rogers, respectively.

A number of conclusions can be taken from these data. The ratio $(\bar{\mu}_{en}/\rho)$ for water to graphite for ^{60}Co radiation changes by no more than 0.2% in going from an in-air irradiation to in-phantom at a depth of 5 cm in a 10×10 cm field. These conditions are consistent with those used for absorbed dose calibrations and therefore would imply that, although the effect of ion-phantom spectrum change is small, it should be considered when precise dosimetry is being carried out but it is not a concern for clinical practice. On the other hand, even if moderately precise measurements are to be made using very large field sizes, the ratio $(\bar{\mu}_{en}/\rho)_{gr}^{water}$ may differ by 2% or more from that applying to in-air measurements and this should be considered. Very similar results are obtained for other materials, such as polymethyl methacrylate (PMMA), polystyrene, and nylon.

Table I also gives the results when this quantity is calculated for muscle tissue to water and bone to water. It shows that there is no appreciable difference for tissue (0.2%) but that $(\bar{\mu}_{en}/\rho)_{water}^{bone}$ differs by over 6% from a point near the surface in a small field to a point 20 cm deep in a 20×20 cm beam and over 15% to this depth in a very large beam.

Bremsstrahlung spectra

A number of bremsstrahlung spectra were also used in the way just described to examine the dependence of $(\bar{\mu}_{en}/\rho)$ on field size and depth. The spectra that were used are taken from those used by Johns and Cunningham² (Tables 7-2 and 7-4), and are cited in that reference. They include 250-kVp, 6-, 12-, 18-, and two different 26-MV spectra, and a 45-MV spectrum. Those used with energies greater than that of ^{60}Co are shown in Figs. 3(a) and 3(b). The graphs show photon energy fluence plotted against photon energy $h\nu$. All of these graphs are normalized to give an integrated energy fluence of 1000; that is, the area under each curve is the same.

An illustrative sample set of the spectra at depths in a phantom is shown in Fig. 4. For this presentation, 6 MV has been chosen because it illustrates the trends which, although less pronounced, are qualitatively the same at higher energies. Figure 4(a) shows the incident energy fluence spectrum and calculated spectra for a 100-cm^2 field area for depths of 0, 5, 10, and 20 cm in the water phantom. The incident spectrum shape is taken from Bentley.⁹ Its shape was determined experimentally. For this calculation, 10^6 photon histories were generated, their initial energies being distributed in 120 energy bins according to the shape shown. The spectra at the depths shown are as calculated; they have not been renormalized. Two changes in the spectrum shape may be noted to occur with depth; there is a relative increase in low-energy photons but at the same time the peak of the spectrum moves slightly to the right. The former is due to production of multiply scattered photons and the latter is the result of the hardening of the primary beam. Neither of these effects is strong and the change in spectral shape with depth is not great.

The change with field size is shown in Fig. 4(b) and is much more dramatic. There is, of course, no hardening of the primary beam, only a buildup of scattered photons.

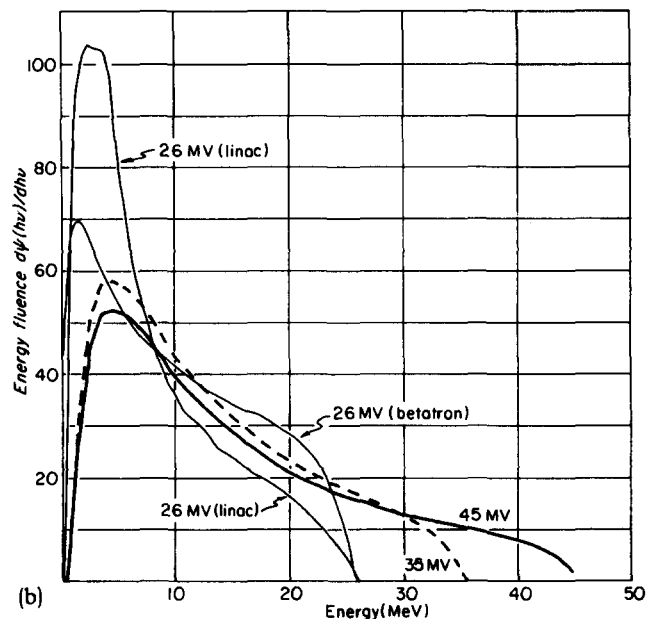
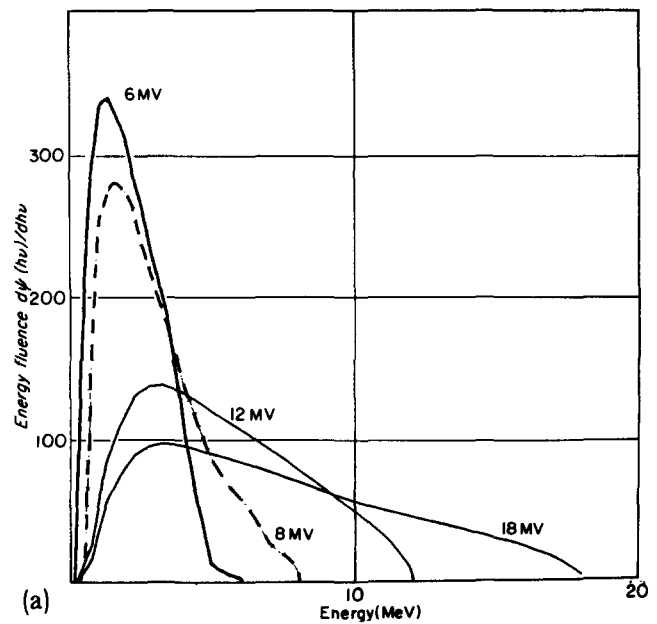


FIG. 3. (a) Input energy fluence spectra for 6 to 18 MV bremsstrahlung radiation used for calculations of absorption coefficient and stopping power ratios. Johns and Cunningham (Ref. 2) and the AAPM dosimetry protocol (Ref. 3). The spectra are normalized to give the same area under each curve. (b) Energy fluence spectra as in part (a) but for 26 to 45 MV.

Again the spectra are plotted as calculated for 10^6 photon histories. The buildup of low-energy photons is now very obvious. By binning scattered photons separately it has been determined that this buildup is indeed due to multiply scattered photons. The amount of this buildup and the lowness of the energies represented is perhaps surprising. As will be seen, this does have an effect on the ratios of mass energy absorption coefficients. A note of interest is the sharp peak which can be seen at an energy of 0.51 MeV and is due to

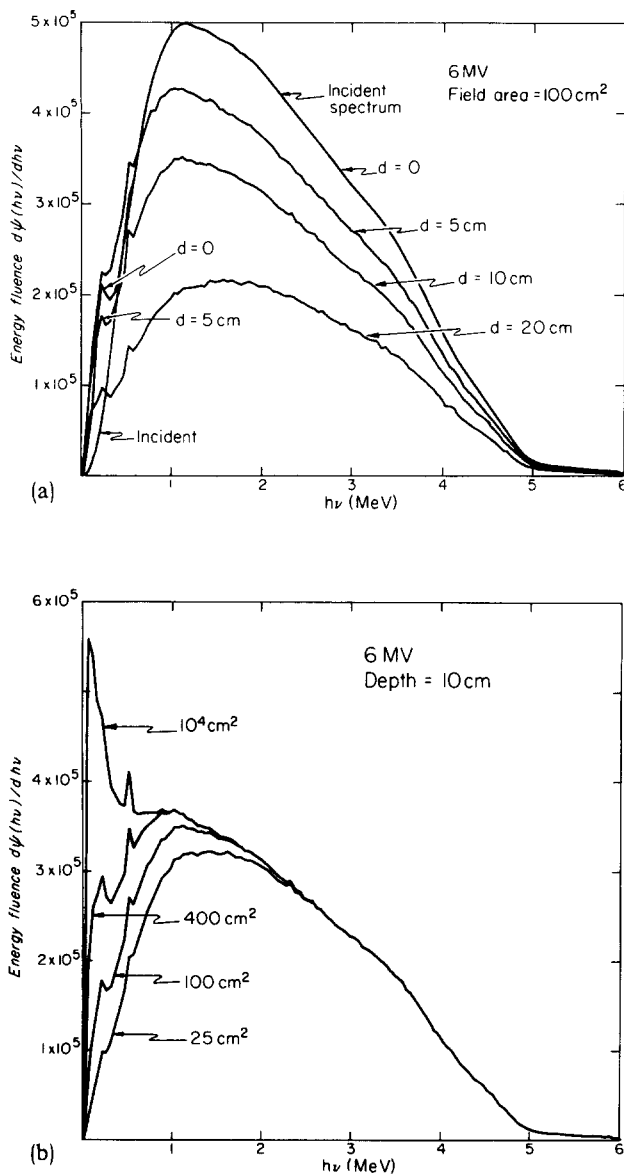


FIG. 4. (a) EGS calculated spectra in a water phantom irradiated by the 6-MV spectrum shown in Fig. 3(a). The five spectra are the incident spectrum and that for depths of 0, 5, 10, and 20 cm, respectively. They show the rather slight change of spectrum shape as the depth is varied. The energy fluence scale refers to a total of 10^6 photon histories. (b) EGS calculated spectra as in (a) but showing the effect, at a depth of 10 cm, of varying the field size from a small beam 5×5 cm in cross section to a large one about 1 m square. The buildup of low-energy photons can be clearly seen. All curves refer to 10^6 photon histories.

annihilation photons. This is seen in all of the high-energy spectra and increases as the field size increases.

In order to illustrate further the change in the spectrum, a number of parameters have been calculated for each of these spectra. Two of them are shown in Table II. Part (a) shows the mean energy of the spectrum for each of the conditions. Part (b) shows the dose weighted mean energy. This is the mean formed by weighting each energy by its spectral value and its mass energy absorption coefficient for water,

$$\hat{E} = \frac{\sum_i [\Delta\phi(h\nu_i)/\Delta h\nu] [\mu_{en}(h\nu_i)/\rho] (h\nu_i)^2}{\sum_i [\Delta\phi(h\nu_i)/\Delta h\nu] [\mu_{en}(h\nu_i)/\rho] h\nu_i}$$

TABLE II. Mean energy and dose weighted energy for 6-MV bremsstrahlung spectra.

Depth	Area (cm ²)			
	25	100	400	∞
(a) Mean energy (MeV) for incident spectrum = 1.45				
0	1.36	1.29	1.19	1.03
5	1.31	1.14	0.96	0.75
10	1.37	1.15	0.91	0.65
20	1.50	1.23	0.91	0.57
(b) Dose weighted mean energy for incident spectrum = 1.97				
0	1.95	1.93	1.90	1.86
5	1.93	1.86	1.79	1.69
10	1.99	1.89	1.77	1.62
20	2.14	2.00	1.82	1.56

This parameter was chosen because it could be expected to be an energy that might be representative of dosimetric parameters such as those in Eq. (3).

The data in the table show that the mean and dose weighted mean energies decrease and then may increase as depth increases and that the energies always decrease as field size increases. These trends are not surprising but the degree of change probably is. Additional calculations showed that these trends should also be expected by analyzing the behavior of primary and once-scattered photons only. By far, the dominant change in the spectrum is the marked increase in the number of photons having energies less than about 0.3 MeV. These photons almost form a satellite spectrum as can be seen in Fig. 4(b). It is a trend that appears in all of the spectra examined.

Ratios of averaged mass energy absorption coefficients for several materials and for a number of spectra as determined by the Monte Carlo calculations for the above set of depths and field sizes are given in Table III. For comparison, the values calculated by Johns and Cunningham,² using only the input spectra, are included in parentheses. These, in every case are equal to or very nearly equal to the numbers obtained from the Monte Carlo calculations for small field sizes and depths. The data in this table show that for high-energy bremsstrahlung spectra and for materials used in the construction of ion chambers, the absorption coefficient ratios do not vary by a significant amount as depth in a phantom or field size is changed. The material showing the largest variation, with respect to water, is graphite where for 6 MV the variation from small fields and shallow depths to an extremely large field is about 0.5%.

The situation is quite different for conventional energy x rays, here represented by 250 kVp (taken from Ref. 2), where variations of almost 10% can be seen in merely going from the surface for a small field to a depth of 10 cm in a 10×10 cm beam. This observation strongly suggests that much previous and present dosimetry with conventional energy x rays is in error. This suggestion is supported by recent calorimetric work by Kubo.¹⁰ It would apply to depth doses and tissue-air ratios¹¹ as well as to factors used in calibrations.

TABLE III. Ratios* of average mass energy absorption coefficients for various energies, depths, and field sizes for different materials.

Beam	Depth	Field radius	$(\bar{\mu}_{en}/\rho)_{med}^{water}$			$(\bar{\mu}_{en}/\rho)_{water}^{med}$	
			Graphite	PMMA	Polystyrene	Muscle	Bone
250 kVp	0	2.8	1.184	1.074	1.107	0.998	1.493
	10	5.6	1.251	1.112	1.173	1.004	1.875
	20	11.3	1.361 (1.155)	1.171 (1.056)	1.282 (1.076)	1.011 (0.995)	2.403 (1.294)
6 MV	0	2.8	1.115	1.031	1.035	0.991	0.960
	10	5.6	1.116	1.031	1.036	0.991	0.975
	20	11.3	1.120 (1.112)	1.034 (1.030)	1.040 (1.035)	0.992 (0.991)	1.019 (0.959)
12 MV	0	2.8	1.122	1.038	1.049	0.990	0.979
	10	5.6	1.123	1.038	1.049	0.990	0.982
	20	11.3	1.124 (1.120)	1.039 (1.039)	1.050 (1.049)	0.990 (0.990)	0.991 (0.979)
18 MV	0	2.8	1.128	1.044	1.059	0.989	0.992
	10	5.6	1.128	1.044	1.059	0.990	0.995
	20	11.3	1.129 (1.125)	1.045 (1.044)	1.060 (1.059)	0.990 (0.989)	1.002 (0.993)
26 MV (thin)	0	2.8	1.129	1.047	1.065	0.990	1.004
	10	5.6	1.131	1.048	1.066	0.990	1.010
	20	11.3	1.134 (1.129)	1.050 (1.049)	1.069 (1.067)	0.989 (0.990)	1.025 (1.005)
26 MV (thick)	0	2.8	1.126	1.043	1.058	0.990	0.991
	10	5.6	1.128	1.044	1.059	0.990	0.996
	20	11.3	1.130 (1.124)	1.046 (1.044)	1.061 (1.058)	0.990 (0.990)	1.009 (0.991)
45 MV	0	2.8	1.141	1.058	1.085	0.989	1.026
	10	5.6	1.140	1.058	1.085	0.989	1.027
	20	11.3	1.141 (1.137)	1.059 (1.059)	1.085 (1.085)	0.988 (0.989)	1.032 (1.027)

*The values in parentheses are from Ref. 2.

When higher atomic number materials are involved, if accurate dosimetry is required, it is clearly necessary to consider the spectral changes and their effect on ratios of mass energy absorption coefficients. This is illustrated by the data on the absorption coefficient ratio for bone to water, where even for 6-MV radiation the change is about 3% in going from a depth of 10 cm in a 10×10 cm beam to 20 cm in a 20×20 cm beam. All of these changes decrease as the energy is increased.

DISCUSSION AND CONCLUSIONS

Ratios of averaged mass energy absorption coefficients have been calculated for a number of photon spectra covering a wide range of energies with the intent of evaluating the importance of the alterations in the spectral composition of the beam as it interacts with an absorbing medium. It has been determined that the ratio that would apply at a point *P* in a phantom is affected principally by the size of the irradiation beam that is used and to a smaller extent by the depth of the point in the phantom. The variation is, as would be ex-

pected, greatest at low energies and least at high energies, and in some situations should be taken into account for dosimetry purposes.

At conventional energy x rays, the ratio of $(\bar{\mu}_{en}/\rho)_{gr}^{water}$ is almost 15% different at a depth of 20 cm in a 20×20 cm beam that it is at or near the surface in a 5×5 cm beam. The clear implication is that these quantities should be included in the determination of percentage depth doses. The lack of this information in the past has almost certainly led to errors of as much as 10% in depth dose values and general dose determinations.

The variation in this quantity for ⁶⁰Co radiation has already been documented^{2,3} but more detail is presented here. There is a clear implication for in-air calibration of cobalt units and for the subsequent use of tissue-air ratios, since determinations of dose both in air and in a phantom are involved and the spectrum at the point of measurement for these two situations will be sufficiently different to cause a difference of up to 0.5% in the absorption coefficient ratios for quite ordinary field sizes but would differ by possibly 2% for the field sizes used for total body irradiation.

Except for orthovoltage energies, no adjustment would be required for percentage depth doses or tissue-phantom ratios, since for these quantities only the depth is changed and the effect on absorption coefficient ratios is small. Also, for energies higher than that from about 6 MV, it is likely that this effect, although still perceptible, can be ignored.

It is not easy to assess the accuracy of these calculations since no independent comparison is available. The input data for mass energy absorption coefficients used here are those due to Hubbell.¹² The data used by Johns and Cunningham² were produced by Plechaty *et al.*¹³ These two sets of data differ by up to 13% for graphite, for example, for photons with energies between 10 and 100 keV, the newer Hubbell¹² values being larger. Similar but somewhat smaller differences are observed for the other materials being considered here. Because we are calculating ratios, and in fact ratios of averaged values, the effects are much diminished even though observed changes in the spectrum are in this energy range. For example, $(\bar{\mu}_{en}/\rho)_{gr}^{water}$ using the Hubbell data is, even for orthovoltage spectra, within 0.2% of the same quantity produced using the Plechaty data. It may be assumed that this is an indication of the uncertainty due to difference in the resource data.

Uncertainties in the details of the incident spectra are a much greater source of error. Unfortunately, it is quite rare that the photon spectrum of a radiation beam being used is known. To choose a value for the absorption coefficient ratio, people have most commonly chosen, somewhat arbitrarily, a representative single energy and from that determined the absorption coefficient ratio. An estimate of the range of uncertainty that this might induce at high energies can be obtained by noting the differences between the two 26-MV spectra in Fig. 3(b). This is really quite an extreme difference and yet $(\bar{\mu}_{en}/\rho)_{gr}^{water}$ differs by no more than 0.5%.

For cobalt radiation the spectra are rather well known and uncertainties should be more related to the input data and ±0.2% should be reasonable. For conventional energies, the variation in absorption coefficient ratio concerned with

variations in spectra, as shown by Johns and Cunningham² for 270-kVp radiation, can be more than 10%. In this energy range, if precision is required, a knowledge of the spectrum is really quite necessary. For all our calculations more than 10^4 photon histories were used. Because we are determining a ratio of two quantities determined from the same set of histories, it is unlikely that photon statistics play any role in producing errors.

The absorption coefficient ratio was chosen for examination because some preliminary calculations, such as with the two spectra for ^{60}Co radiation,² suggested that this is the dosimetric quantity that might be the most sensitive to photon spectrum composition. It is not yet clear whether variations in other parameters will be significant.

ACKNOWLEDGMENTS

This work was in part supported by grants from the Ontario Cancer Treatment and Research Foundation and the National Cancer Institute of Canada. We also wish to acknowledge many discussions with Mr. J. Van Dyk, Mr. J. A.

Rawlinson, and other members of the Clinical Physics group of the Ontario Cancer Institute, and Dr. H. E. Johns.

¹W. R. Nelson, in *Computer Techniques in Radiation Transport and Dosimetry*, edited by W. R. Nelson and T. M. Jenkins (Plenum, New York, 1980).

²H. E. Johns and J. R. Cunningham, *The Physics of Radiology*, 4th ed. (Thomas, Springfield, IL, 1983).

³Task Group 21, Radiation Therapy Committee, AAPM, *Med. Phys.* **10**, 741 (1983).

⁴R. Loevinger, *Med. Phys.* **8**, 1 (1981).

⁵J. R. Cunningham and R. J. Schulz, *Med. Phys.* **11**, 618 (1984).

⁶W. R. Bruce and H. E. Johns, *Br. J. Radiol. Suppl.* **9** (1960).

⁷D. W. O. Rogers, A. F. Bielajew, and G. M. Ewart, *Med. Phys.* **11**, 401 (1984).

⁸D. W. O. Rogers, *Nucl. Instrum. Methods* **199**, 531 (1982).

⁹R. E. Bentley, J. C. Jones, and S. C. Lillicrap, *Phys. Med. Biol.* **12**, 301 (1967).

¹⁰H. Kubo, *Radiother. Oncol.* **4**, 275 (1985).

¹¹D. K. Bewley, A. L. Bradshaw, J. E. Burns, M. Cohen, M. J. Day, T. J. Godden, D. Greene, W. A. Jennings, S. C. Lillicrap, C. W. Smith, and P. C. Williams, *Br. J. Radiol. Suppl.* **17** (1983).

¹²J. H. Hubbell, *Int. J. Appl. Radiat. Isot.* **33**, 1269 (1982).

¹³E. F. Plechaty, D. E. Cullen, and R. J. Howerton, UCRL Report No. 50400, Vol. 6, Revision 1, 1975.